J. Fluid Mech. (2004), *vol.* 519, *pp.* 359–376.
DOI: 10.1017/S0022112004001296 Printed in the United Kingdom

On the motion of bubbles in vertical tubes of arbitrary cross-sections: some complements to the Dumitrescu–Taylor problem

By CHRISTOPHE CLANET, PIERRE HÉRAUD AND GEOFFREY SEARBY

Institut de Recherche sur les Phénomènes Hors Equilibre, UMR 6594, 49 rue F. Joliot Curie B.P. 146, 13384 Marseille, France

(Received 3 June 2003 and in revised form 12 July 2004)

We first study the rising velocity U_b of long bubbles in vertical tubes of different cross-sections, under the acceleration due to gravity g. The vessel being initially filled with a liquid of kinematic viscosity ν, it is known that for cylindrical tubes of radius R, high-Reynolds-number bubbles ($Re \equiv U_b R/\nu \gg 1$) are characterized by Newton's law $U_b \propto \sqrt{gR}$ and low-Reynolds-number bubbles by Stokes' law $U_b \propto gR^2/\nu$. We show experimentally that these results can be generalized for vessels of 'arbitrary' cross-section (rectangles, regular polygons, toroidal tubes). The high-Reynolds-number domain is shown to be characterized by $U_b = (8\pi)^{-1/2}\sqrt{gP}$, and the low-Reynolds-number range by $U_b \approx 0.012gS/\nu$, where P and S respectively stand for the wetted perimeter and the area of the normal cross-section of the tube. We derive an analytical justification of these results, using the rectangular geometry. Finally, the problem of long bubble propagation in an unsteady acceleration field is analysed. The theory is compared to existing data.

1. Introduction

Dumitrescu–Taylor bubbles derive their name from the two landmark papers by Dumitrescu (1943) (a student of L. Prandtl) and Davies & Taylor (1950). Both studies were mainly motivated by the development of submarine technology and consider the propagation of a long air bubble in a vertical cylindrical tube, initially filled with a low-viscosity liquid (such as water). Other applications, such as oil extraction have also initiated the study of bubbles rising in viscous liquids (Saffman & Taylor 1958; Bretherton 1961). For a general review on long bubble propagation, see Fabre & Liné (1992). More recently, the development of biomechanics and microfluidic devices have induced an interest in the problem of bubble propagation in 'small' tubes with non-circular cross-sections (Kolb & Cerro 1995; Bi & Zhao 2001; Hazel & Heil 2002; Liao & Zhao 2003).

The problem we address is sketched in figure 1(*a*). A large air bubble rises into a vertical tube of arbitrary cross-section, initially filled with a liquid characterized by its density ρ, kinematic viscosity ν and surface tension σ. The motion of the bubble is driven by the acceleration due to gravity g and is characterized by a constant velocity U_b. The problem is to determine the relation between the rising velocity U_b and the shape of the tube, knowing the liquid properties.

In the case of cylindrical tubes, $R(\theta) = R$, different regimes of propagation have been identified. In the limit of high Reynolds number, $Re \equiv U_b R/\nu \gg 1$, and weak

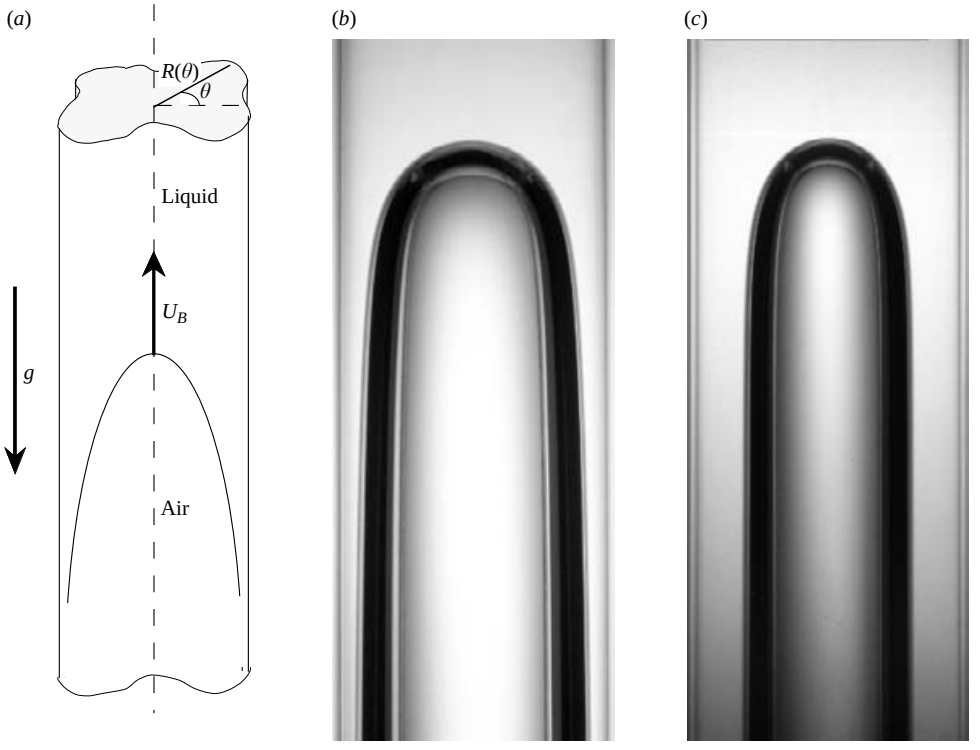

FIGURE 1. (*a*) Presentation of the problem, (*b*) air bubble propagating in a cylindrical tube 78 mm in diameter in water, (*c*) air bubble propagating in the same tube, but through silicone oil V12500.

curvature, Dumitrescu showed both theoretically and experimentally that:

$$U_b = \lambda\sqrt{gR} \quad \text{with} \quad \lambda \approx 0.5. \tag{1.1}$$

Dumitrescu also studied the influence of the curvature of the interface, observing the propagation of bubbles in tubes whose diameter is comparable with the capillary length $a \equiv \sqrt{\sigma/(\rho g)}$. His experimental results for air bubbles in water showed that equation (1.1) only applies in the limit $R/a > 4$. Below this limit, λ is no longer constant but decreases as the Bond number, $Bo \equiv R/a$, decreases.

Experimentally, the most extensive studies on long bubbles in cylindrical tubes are those of Zukoski (1966) and of White & Beardmore (1962). They both confirm Dumitrescu's results on the effect of curvature and show that viscous effects are negligible when $Re > 200$. At low Reynolds numbers $Re < 1$, White & Beardmore (1962) showed that:

$$U_b = \alpha\frac{gR^2}{\nu} \quad \text{with} \quad \alpha \approx 0.038. \tag{1.2}$$

This value of α is constant in the limit $R/a \gg 1$, but decreases with decreasing R/a when this latter is of order unity. More recently, particle image velocimetry techniques have been used to study the velocity field around large bubbles (Bugg & Saad 2002; van Hout *et al.* 2002).

The problem of bubble propagation in narrow cylindrical tubes has been addressed experimentally (Taylor 1961; Aussillous & Quéré 2000), theoretically (Bretherton

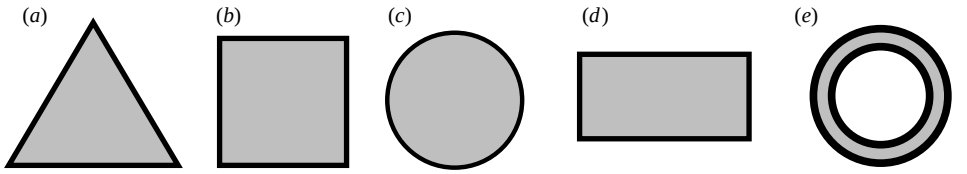

FIGURE 2. Different tube cross-sections used to study the propagation of long air bubbles.

1961; Park & Homsy 1984; Ratulowski & Chang 1989) and numerically (Reinelt & Saffman 1985; Reinelt 1987).

Bubble propagation in non-axisymmetric tubes has received much less attention. Moreover, the studies are mainly motivated by microfluidic, imbibition or biofluidic applications and focus on narrow tubes either experimentally (Kolb & Cerro 1991, 1993, 1995; Bico & Quéré 2002), theoretically (Wong, Radke & Morris 1995*a*, *b*) or numerically (Hazel & Heil 2002).

Here, we first focus on the propagation of large bubbles (large compared to the capillary length) in vertical tubes of arbitrary cross-section. The experimental set-up is presented in § 2 prior to the experimental results in § 3. Models for the high- and low-Reynolds-number regimes are given in § 4. Finally, the unsteady dynamics of long bubbles in vertically shaken tubes is analysed in § 5 before the conclusion.

2. Experimental set-up

2.1. *The synopsis*

The experimental set-up reduces to a vertical transparent PVC tube, initially filled with a Newtonian liquid. The tube is closed at the top and at the bottom. At $t = 0$, the bottom is rapidly removed. We then record the motion of the air bubble using a video camera. Typical bubble shapes are presented in figure 1(*b*, *c*). The air bubble propagates through water in figure 1(*b*) and through V12500 silicone oil in figure 1(*c*). In both cases, the tube is cylindrical, 78 mm in diameter. These images are digitized at 25 f.p.s. using a Canon XM2 video camera. MATLAB is used for image processing. The out-flowing liquid falls into a reception tank and is re-used after a degassing period, the duration of which increases with liquid viscosity.

2.2. *The tubes*

All the tubes used in this study have a high length to perimeter ratio (typically 10). To avoid end effects, our measurements are conducted in the central area, defined as one perimeter away from both the entrance and the end. In this region, the bubble velocity is constant and only depends on the fluid properties and on the shape of the cross-section of the tube.

To study the influence of the shape of the tube on the terminal velocity of long bubbles, we have used the five classes of cross-section presented in figure 2.

2.3. *The liquids*

As stated in § 1, previous studies have shown that in the large-Reynolds-number limit, the bubble velocity in cylindrical tubes scales as $U_b \propto \sqrt{gR}$. In the low-Reynolds-number limit ($U_b R/\nu \ll 1$), the dependency on the tube radius R is changed to $U_b \propto gR^2/\nu$. Equating both expressions, shows that the transition between both regimes occurs for a tube radius $R \propto l_\nu$ where $l_\nu \equiv (\nu^2/g)^{1/3}$. This transition is not affected by surface tension provided that l_ν is large compared to the capillary length

Liquid	ρ (kg m^{-3})	ν (m^2 s^{-1})	σ (kg s^{-2})	a (m)	Ka
Ether	705	0.32×10^{-6}	0.0173	1.6×10^{-3}	72
Pentane	623	0.37×10^{-6}	0.0162	1.6×10^{-3}	68
Hexane	653	0.46×10^{-6}	0.0184	1.7×10^{-3}	61
Water	993	10^{-6}	0.0700	2.7×10^{-3}	57
Ethanol	785	1.47×10^{-6}	0.0215	1.7×10^{-3}	28
SO V5	913	5×10^{-6}	0.0225	1.6×10^{-3}	12
SO V20	942	2×10^{-5}	0.0225	1.6×10^{-3}	4.5
SO V50	948	5×10^{-5}	0.0225	1.6×10^{-3}	2.5
SO V100	952	1×10^{-4}	0.0225	1.6×10^{-3}	1.5
SO V300	952	3×10^{-4}	0.0225	1.6×10^{-3}	0.7
Glycerol	1260	9×10^{-4}	0.063	2.25×10^{-3}	0.52
SO V1000	965	10^{-3}	0.0225	1.5×10^{-3}	0.3
SO V12500	965	1.25×10^{-2}	0.0225	1.5×10^{-3}	0.06
SO V100000	965	0.1	0.0225	1.5×10^{-3}	0.02

TABLE 1. Physical properties of the different Newtonian liquids used (at 25 °C).

$a\equiv\sqrt{\sigma/(\rho g)}$. The ratio of these two lengths is the Kapitsa number†:

$$Ka\equiv\frac{a}{l_\nu}=\left(\frac{\sigma^3}{\rho^3 g\nu^4}\right)^{1/6}. \tag{2.1}$$

In a given gravitational field, this number depends only on the physical properties of the liquid. For example, for water on earth, $Ka\approx57$. This large value implies that with water, the reduction of the tube radius will first reveal capillary effects prior to viscous ones. Thus, water cannot be used to study the transition from high to low Reynolds numbers without capillary effects.

To study the influence of the liquid we have used the different Newtonian liquids presented in table 1. For each liquid, we give, from left to right, its density ρ (kg m^{-3}), kinematic viscosity ν (m^2 s^{-1}), surface tension σ (kg s^{-2}), capillary length (m) and the Kapitsa number. From ether to V5, the Kapitsa number is larger than 10 and the different liquids are characterized by low viscosities and different surface tensions. To reach the low-Kapitsa-number region, we have used glycerol and Rhodorsil silicone oils (SO). The latter allows a variation of the viscosity over five decades with a constant surface tension.

3. First experimental results

To follow the tradition of studies in hydraulics, we first present our experimental results using the hydraulic radius $R_H\equiv2A/P$, defined as twice the ratio between the cross-section area A and the wetted perimeter P.

3.1. *Taylor bubbles at large Reynolds and large Bond numbers*

We work here with air bubbles at high Reynolds number and quantify their propagation in vertical tubes with dimensions much larger then the capillary length.

† In the literature, this non-dimensional number is often called the Morton number, following Haberman & Morton (1956). However, as mentioned in Fulford (1964), Kapitsa (1948) first introduced this dimensionless quantity in his study on the flow of thin films.

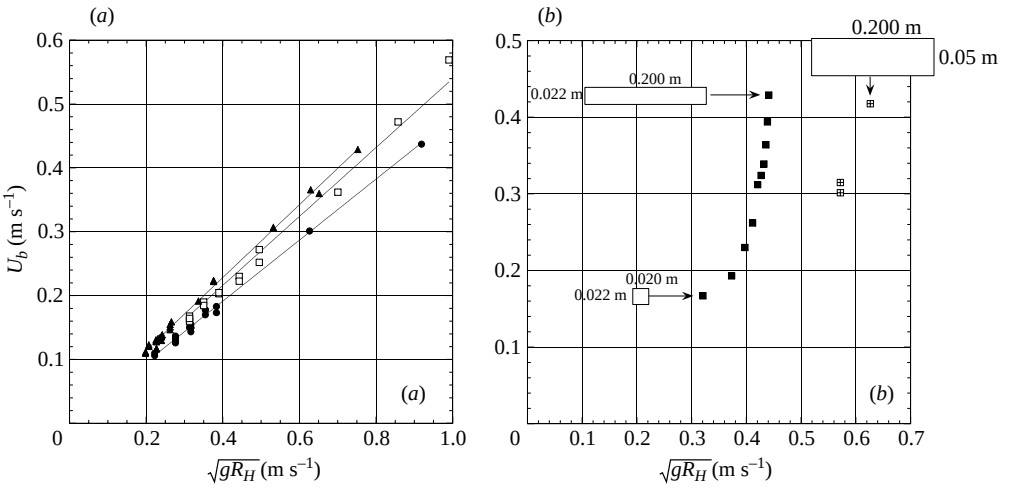

FIGURE 3. Experimental results obtained at high-Reynolds number with high-Kapitsa-number liquids. (*a*) Evolution of the bubble velocity U_b with the tube radius $\sqrt{gR_H}$ in regular polygons: ▲, triangles; □, squares; ●, circles; the solid lines indicate the best linear fits $U_b = Fr_H\sqrt{gR_H}$. For triangles, squares and circles, we find $Fr_H = 0.6$, $Fr_H = 0.54$ and $Fr_H = 0.48$, respectively. (*b*) Evolution of the bubble velocity U_b with the tube radius $\sqrt{g}R_H$ in tubes of rectangular section: ■, the width is constant and equal to 2.2 cm; ⊞, the width is constant and equal to 5 cm.

The evolution of the velocity U_b obtained with high-Kapitsa-number liquids in tubes of different cross-sections is presented in figure 3. For regular polygons, figure 3(*a*) shows that U_b is a linear function of $\sqrt{gR_H}$. However, the proportionality constant, $Fr_H \equiv U_b/\sqrt{gR_H}$, depends on the shape. A linear regression on the different data sets shows that Fr_H is 0.6 for triangles, 0.54 for squares and 0.48 for circles. This latter value is fully compatible with previous studies, mentioned in § 1.

The evolution of U_b with $\sqrt{gR_H}$ obtained in rectangles is presented in figure 3(*b*). For a given width, a strong nonlinear dependence is observed as the size of the rectangle is increased. Moreover, it is evident that the same bubble velocity can be obtained in tubes of different hydraulic radii. We come back to this problem in § 4.

3.2. *Taylor bubbles at low Reynolds and large Bond numbers*

We work here with air bubbles at low Reynolds number in liquids characterized by Kapitsa numbers smaller than unity and quantify their propagation in vertical tubes with dimensions much larger than the capillary length.

The evolution of the velocity U_b obtained with silicone oils in tubes of different cross-sections is presented in figure 4. For regular polygons, we observe in figure 4(*a*) that U_b is still a linear function of gR_H^2/ν. However, the proportionality constant, $St_H \equiv U_b\nu/(gR_H^2)$, depends on the shape. The linear regression performed on the different data sets show that St_H is 0.055 for triangles, 0.043 for squares and 0.035 for circles. This latter value is consistent with previous studies mentioned in § 1.

The evolution of U_b with gR_H^2/ν obtained with rectangles is presented in figure 4(*b*). For a given width, the increase of the rectangular cross-section leads to a nonlinear evolution of the bubble velocity. Moreover, the evolutions obtained with two different widths do not superpose.

These observations concerning the bubble velocity in regular polygons and rectangles are similar to the observations in § 3.1.

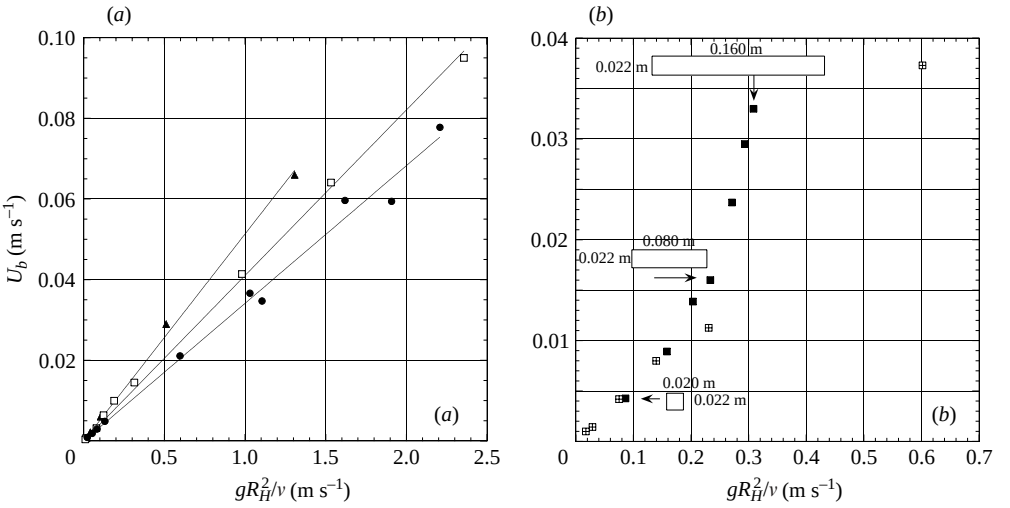

FIGURE 4. Experimental results obtained with silicone oils V1000, V12500 and V100000. (*a*) Evolution of the bubble velocity U_b with the velocity gR_H^2/ν in regular polygons: ▲, triangles; □, squares; ●, circles; the solid lines are the best linear fits $U_b = St_H gR_H^2/\nu$. For triangles, squares and circles, we find, respectively, $St_H = 0.055$, $St_H = 0.043$ and $St_H = 0.035$. (*b*) Evolution of the bubble velocity U_b with the scaling velocity gR_H^2/ν in rectangles: ■, the width is constant and equal to 2.2 cm; ⊞, the width is constant and equal to 4 cm.

4. Models and further experimental results

This section is dedicated to the interpretation of the different experimental results presented in § 3.

4.1. *Taylor bubbles at large Reynolds and large Bond numbers*

In this regime, since the fluid is initially at rest, the motion of the liquid around the bubble is assumed to be potential at all times, following Lagrange's theorem. In the frame of reference moving with the bubble (the apex defining the origin), the flow is steady and the first problem is to solve $\Delta\phi = 0$, where ϕ is the velocity potential ($\boldsymbol{U} = \nabla\phi$). This Laplace equation must be solved with the appropriate boundary conditions: the normal component of the velocity is zero at the walls, the velocity vanishes at the apex and far ahead of the bubble, the velocity is equal to the bubble velocity. If y is the vertical axis pointing in the direction of gravity, the general form of the potential is $\phi(x, y, z) = U_b y + \bar{\phi}(x, y, z)$, where $\bar{\phi}(x, y, z)$ must satisfy the Laplace equation with the same boundary conditions except $\lim_{y\to-\infty} \bar{\phi}(x, y, z) = 0$. Once the function $\bar{\phi}$ is found, for example by separation of variables and series expansion, we observe that any value of U_b will satisfy the condition of constant velocity ahead of the bubble. The velocity is selected by matching the dynamical conditions at the interface.

In the limit of high Reynolds number and in the absence of capillary effects, there is no pressure jump across the gas/liquid interface. The pressure in the liquid along the interface is constant and equal to the pressure in the gas. The projection of the Euler equation onto the interface yields simply $\mathrm{d}U^2 = 2g\mathrm{d}y$. In the reference frame moving with the bubble, the apex is a stagnation point and the above equation can be integrated as:

$$U^2 = 2gy, \tag{4.1}$$

where y is the distance from the apex. The dynamical condition thus imposes that the square of the liquid velocity linearly increases with the axial distance from the apex.

4.1.1. *Axisymmetrical bubbles*

In cylindrical coordinates (radial coordinate r and vertical coordinate y), the velocity potential can be expanded in series, the first terms being:

$$\phi \approx U_b y + A_0 \mathrm{e}^{(k_0 y)} J_0(k_0 r), \tag{4.2}$$

where J_0 is the Bessel function of order 0. The two constants A_0 and k_0 are determined using the two boundary conditions, $u(r = R) = 0$ and $u(0, 0) = v(0, 0) = 0$. Since $\mathrm{d}\, J_0(r)/\mathrm{d}\, r = -J_1(r)$, the condition at the wall is satisfied if $k_0 R = 3.83$, where the value 3.83 corresponds to the first zero of the Bessel function J_1. The condition at the apex leads to $A_0 = -U_b/k_0$.

The associated streamfunction, ψ, is:

$$\psi = \frac{U_b r}{k_0}\left(\mathrm{e}^{(k_0 y)} J_1(k_0 r) - \tfrac{1}{2} k_0 r\right). \tag{4.3}$$

Developing the velocity along the bubble ($\psi = 0$) in the region of the apex ($r, y \ll 1$) shows that the dynamical condition (4.1) is only satisfied with the velocity:

$$U_b^2 = \frac{g}{k_0} \quad \text{or} \quad U_b = \sqrt{\frac{gR}{3.83}} \approx 0.51\sqrt{gR}. \tag{4.4}$$

This evaluation is qualitatively correct, but the numerical value of the constant is between 6% and 10% higher than the numerous experimental results reported for this configuration in the literature by Dumitrescu (1943), Davies & Taylor (1950) and Zukoski (1966). Equation (4.4) was first derived by Layzer (1955). In the domain of flame front propagation in tubes, the same approach was used by Zel'dovich (1980) to analyse the speed of a curved laminar flame. Note that the approach used by Davies & Taylor (1950) is different since they do not match the dynamical condition at the apex, but at some isolated well-chosen points. We now try to generalize (4.4) to tubes characterized by two length scales.

Note that much mathematical and numerical work has been devoted to extending the axisymmetric study to higher-order expansions than (4.2) (Garabedian 1957; Daripa 2000).

4.1.2. *Bubbles in rectangular channels*

An example of an air bubble rising in a rectangular tube is presented in figure 5. In this example, the rectangle width is $2R_x = 14\,\mathrm{cm}$ and its thickness $2R_z = 2.2\,\mathrm{cm}$. The bubble velocity is $U_b = 0.34\,\mathrm{m\,s^{-1}}$. In all the sections dedicated to rectangles, $\boldsymbol{e}_y$ points in the vertical direction towards the air and $\boldsymbol{e}_x$, $\boldsymbol{e}_z$ define the principal axes of the rectangle.

To describe the flow ahead of the bubble, we look for a solution of the Laplace equation, $\Delta\phi = 0$, in the Cartesian coordinate system (x, y, z) under the form:

$$\phi = U_b y + A(R_x, R_z)\mathrm{e}^{ky}\cos(kx) + B(R_x, R_z)\mathrm{e}^{my}\cos(mz). \tag{4.5}$$

This solution is the superposition of the potentials used to describe a two-dimensional planar bubble. As R_z tends to zero, the coefficient B should tend to zero. In the same way, as R_x tends to zero, the coefficient A should vanish so that in both limits the two-dimensional flow will be recovered. We now focus on the determination of the coefficients A and B: the boundary conditions at the walls $u_x(x = R_x, \forall y, \forall z) = 0$

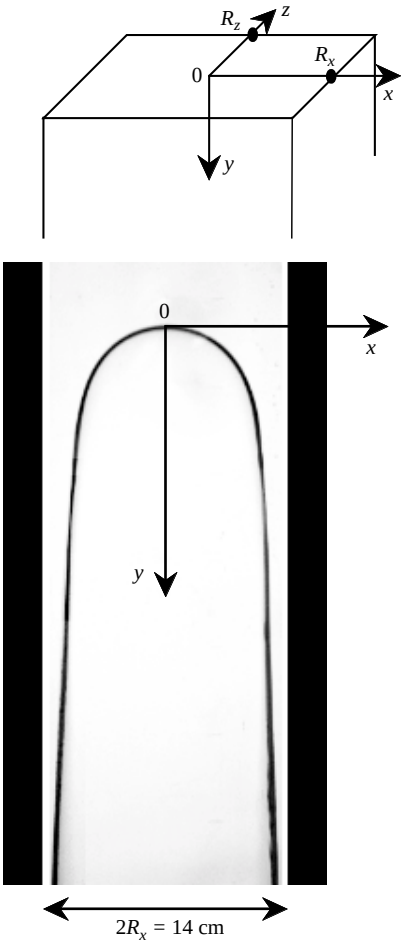

FIGURE 5. Air bubble rising through water in a rectangular tube of width $2R_x = 14\,\text{cm}$ and thickness $2R_z = 2.2\,\text{cm}$.

and $u_z(\forall x, \forall y, z = R_z) = 0$, respectively, imply:

$$k = \pi/R_x, \quad m = \pi/R_z. \tag{4.6}$$

The vanishing of the velocity at the apex $\boldsymbol{U}(0, 0, 0) = 0$ implies:

$$U_b + Ak + Bm = 0. \tag{4.7}$$

At this point, A, B and U_b are the remaining unknowns: as in the previous examples U_b will be deduced from the dynamical condition which must be satisfied at the surface of the bubble. Prior to that, the coefficients A and B must be expressed using the structure of the stagnation point and the symmetries of the problem.

Expanding the velocity field around the apex we obtain:

$$u_x = -Ak^2x, \quad u_z = -Bm^2z, \quad u_y = (Ak^2 + Bm^2)y - Ak^3x^2/2 - Bm^3z^2/2. \tag{4.8}$$

The streamlines are defined by the differential equations:

$$\frac{\mathrm{d}x}{u_x} = \frac{\mathrm{d}y}{u_y} = \frac{\mathrm{d}z}{u_z}. \tag{4.9}$$

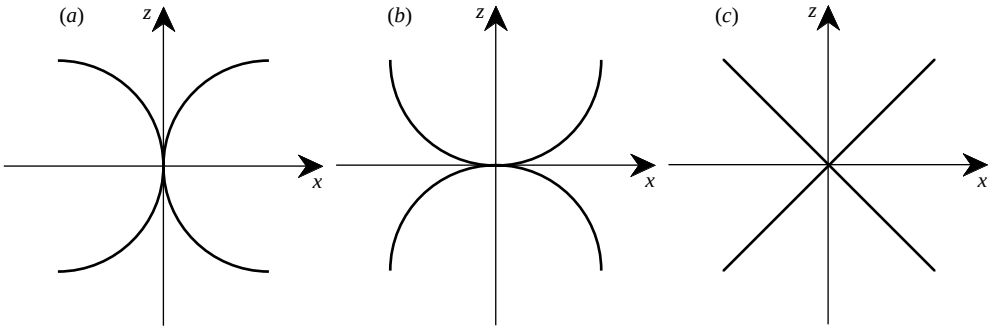

FIGURE 6. Different shapes of the streamline depending on α: (*a*) $\alpha > 1$; (*b*) $\alpha < 1$; (*c*) $\alpha = 1$.

According to (4.8), the streamlines at the apex in the (x, z)-plane can be expressed as:

$$\frac{\mathrm{d}x}{Ak^2x} = \frac{\mathrm{d}z}{Bm^2z}, \tag{4.10}$$

which describes a power-law dependency $x = z^\alpha$ with $\alpha \equiv Ak^2/Bm^2$. Looking at the derivative, $\mathrm{d}x/\mathrm{d}z = \alpha z^{\alpha-1}$, we see that if $\alpha < 1$ (figure 6*b*), the derivative $(\mathrm{d}x/\mathrm{d}z)_{z=0}$ is infinite so that the z-axis, defined by $x = 0$, does not receive any liquid. In the same way, if $\alpha > 1$ (figure 6*a*), the x-axis is not fed. The isotropic repartition of liquid thus implies $\alpha = 1$ (figure 6*c*), so that:

$$\frac{Ak^2}{Bm^2} = 1. \tag{4.11}$$

Together with (4.7), this isotropic condition leads to the following expressions for A and B:

$$A = -\frac{m}{k^2 + km}U_b, \quad B = -\frac{k}{m^2 + km}U_b. \tag{4.12}$$

From these expressions, we see that as R_x goes to zero, k goes to infinity and A vanishes as expected. In a symmetrical way, as R_z goes to zero, m goes to infinity and B vanishes. The expression for the velocity potential is thus:

$$\phi = U_b\left[y - \frac{m}{k^2 + km}\mathrm{e}^{ky}\cos(kx) - \frac{k}{m^2 + km}\mathrm{e}^{my}\cos(mz)\right]. \tag{4.13}$$

If R_x and R_z are interchanged, k and m are interchanged. In this transformation, A and B do transform one into the other so that the velocity potential is unchanged if x and z are interchanged. This symmetry is essential, since it consists in looking at the bubble from the side, a transformation that obviously does not change the flow field or the rising velocity.

In the (x, y)-plane, the streamlines are solutions of the differential equation $\mathrm{d}x/u_x = \mathrm{d}y/u_y$ which can be expanded in the region close to the apex using (4.8):

$$\frac{\mathrm{d}y}{2y - kx^2/2 - mz^2/2} = -\frac{\mathrm{d}x}{x}. \tag{4.14}$$

Using the relation $z = x/\tan\theta$, where θ is the angle between the z-axis and the streamline in the (x, z)-plane, (4.14) can be integrated:

$$x^2 = \frac{8}{k + m/\tan^2\theta}y. \tag{4.15}$$

In the same way, the streamline in the (y, z)-plane is:

$$z^2 = \frac{8}{k\tan^2\theta + m} y. \tag{4.16}$$

We recover the parabolic structure of the apex that has already been observed for two-dimensional axisymmetrical bubbles.

The dynamical condition which must be satisfied on the surface of the bubble is $U^2 = 2gy$. Expanding the velocity field (4.8) close to the apex, we find:

$$u_y \approx Ak^2(2y - kx^2/2 - mz^2/2), \quad u_x = -Ak^2x, \quad u_z = -Ak^2z. \tag{4.17}$$

From this velocity field and the bubble shape at the apex, we deduce that $U^2 \equiv u_x^2 + u_y^2 + u_z^2 \approx u_x^2 + u_z^2 \approx A^2k^4(x^2 + z^2)$, which is:

$$U^2 = 8A^2k^4y \left[\frac{1}{k + \dfrac{m}{\tan^2\theta}} + \frac{1}{k\tan^2\theta + m} \right]. \tag{4.18}$$

We obtain the necessary linearity between U^2 and y, but U^2 is found to depend on θ. This dependency can be discussed on physical grounds: The two terms inside the brackets stand for the contributions of u_x^2 and u_z^2, respectively. When R_z goes to zero (m goes to infinity), we should find only the contribution of u_x^2. In the same way, when R_x goes to zero (k goes to infinity), we should find only the contribution of u_z^2. This is not the case in (4.18) except for the special angle $\theta^\star$ such that $\tan^2\theta^\star \equiv m/k$ for which:

$$U^2 = 8A^2k^4y \left[\frac{1}{2k} + \frac{1}{2m} \right]. \tag{4.19}$$

The two contributions are now symmetrical and one can vanish independently from the other, which is physically correct. The fact that this decoupling is obtained only for a special angle arises from our truncation of the velocity potential (4.5). Adding more terms in the expansion of the potential should make it possible to verify this condition for all angles. Using the expressions for k and m given in (4.6), and the expression for A from (4.12), the velocity evolves as $U^2 = 4\pi U_b^2 y/(R_x + R_z)$. Matching this expression with $2gy$ thus leads to:

$$U_b = \frac{1}{\sqrt{8\pi}} \sqrt{gP} \approx 0.2\sqrt{gP}, \tag{4.20}$$

where $P = 4(R_x + R_z)$ is the perimeter of the rectangular tube.

Our experimental results for air bubbles rising in rectangular tubes initially full of water are replotted in figure 7. The black squares were obtained keeping the thickness equal to 2.2 cm and increasing the width from 2.2 cm up to 20 cm. The white squares correspond to rectangles of thickness 5.0 cm, width 10.0 cm and 20.0 cm. In figure 7, the dashed line is the velocity predicted by (4.20). This approximation is found to be in close agreement with the measurements performed over a reasonable range of aspect ratios and perimeters. We also observe in this figure the agreement of our results with those obtained in rectangles by other authors (Griffith 1964; Sadatomi & Sato 1982). Sadatomi & Sato try the perimeter as the characteristic length scale: 'in the present study the perimeter was tested as the characteristic dimension'. Here, we have shown how this characteristic length scale can be extracted from Euler's equation.

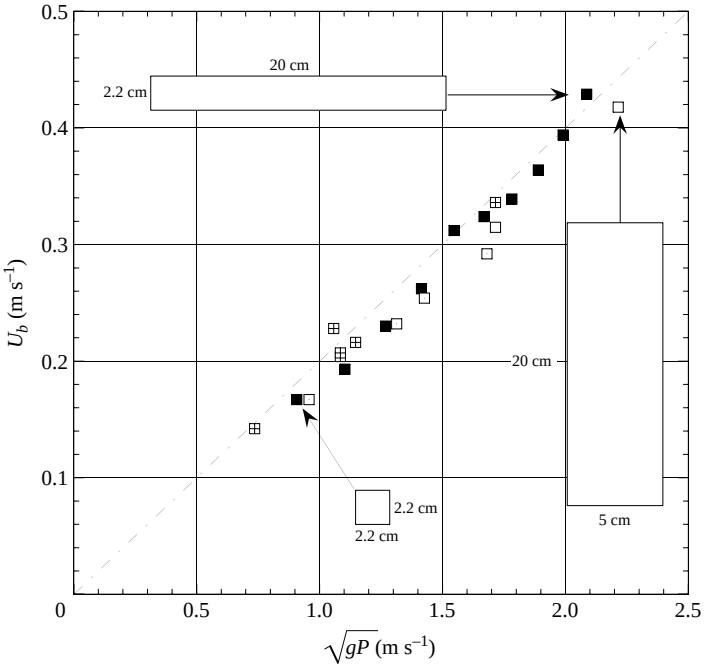

FIGURE 7. Rising velocity of bubbles U_b in rectangular tubes, presented as a function of $\sqrt{gP}$, where $P \equiv 4(R_x + R_z)$ is the perimeter of the rectangle: ■, the thickness is fixed to 2.2 cm; □, the thickness is fixed to 5 cm; ⊡, results in rectangles from Griffith (1964); ⊞, results in rectangles from Sadatomi & Sato (1982); - · -, theoretical estimation provided by (4.20).

4.1.3. *Bubbles in tubes of arbitrary cross-section*

If we use the perimeter $P = 2\pi R$ of a cylindrical tube in the expression $U_b = (8\pi)^{-1/2}\sqrt{gP}$ derived for rectangles, we find $U_b = 1/2\sqrt{gR}$ which is an accurate evaluation of the rising velocity of bubbles in cylindrical tubes.

We now make the assumption that (4.20) is a generalization of the well-accepted result for circular tubes, and is applicable to tubes of arbitrary cross-section.

The results obtained for triangles (△) and squares (■) are presented in figure 8. In this figure, the measured rising velocity U_b on the vertical axis is presented as a function of the scaling velocity $\sqrt{gP}$. For triangles and squares, we observe that U_b is indeed the same linear function of $\sqrt{gP}$, the slope is in close agreement with the law derived for rectangles $U_b = (8\pi)^{-1/2}\sqrt{gP}$ and shown by the dashed line in figure 8.

An intriguing feature of the relation between the velocity and the perimeter is that for a given section, we must increase the perimeter to increase the velocity. The cylinder thus minimizes the velocity for a given section. We have performed an experiment using a toroidal tube of outer diameter 24.1 cm and of inner diameter 15 cm. The bubble we observed in this tube is presented in figure 9. The toroidal bubble in this geometry does not keep a cylindrical symmetry, but is rather wrapped around the central tube as already observed by Hills & Chety (1998). To understand the front/side/back views presented in figure 9, we can imagine a bubble propagating in a rectangular tube that has been bent to form a toroidal tube. An attempt to describe this shape can be found in Das *et al.* (2002). The velocity of the bubble propagating in this tube is plotted in figure 8 with the symbol ⊞. It falls on the same line $U_b = (8\pi)^{-1/2}\sqrt{gP}$ as the triangles, the squares, the rectangles and the cylinders.

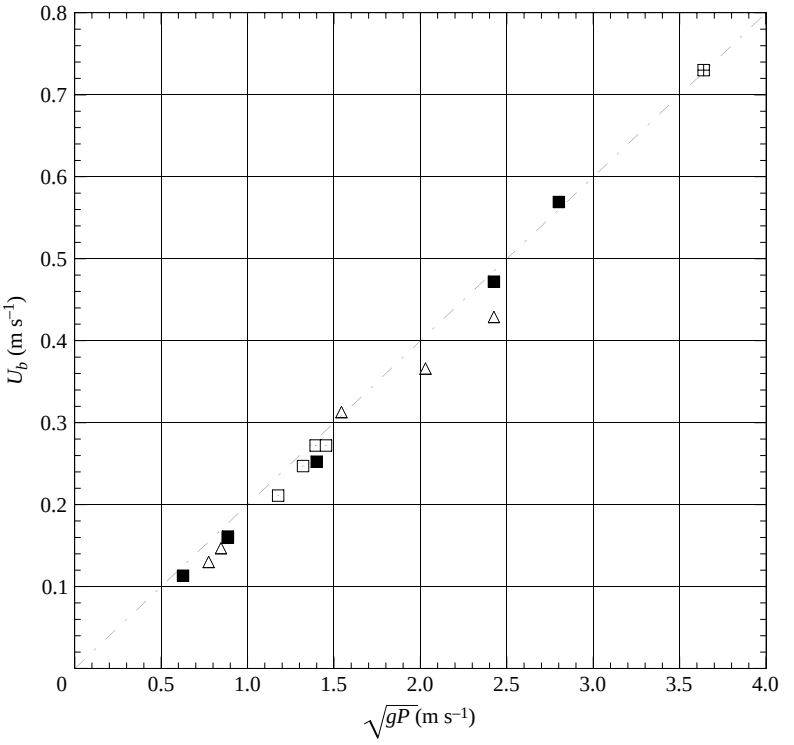

FIGURE 8. Rising velocity of bubbles U_b in triangles (△), squares (■), our toroidal tube (⊞), toroidal tubes from Sadatomi & Sato (1982) (⊡). - · -, theoretical estimate provided by (4.20).

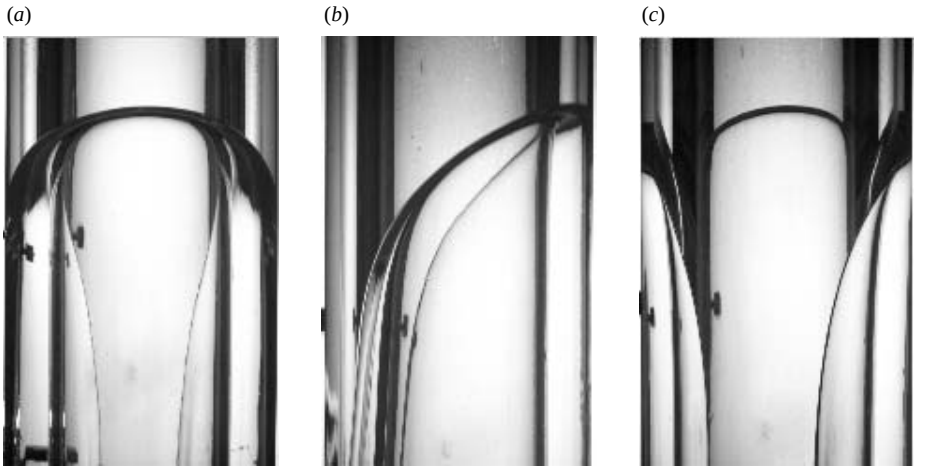

FIGURE 9. Toroidal bubble with water visualized in a tube of internal diameter 15.0 cm and external diameter 24.1 cm: (*a*) front view; (*b*) side view; (*c*) back view.

We underline here that the dynamics of Taylor bubbles in a torus is important since such bubbles occur in riser tubes of gas and oil wells during drilling and logging operations or in double pipe heat exchangers where vaporization is important. Das *et al.* (1998) provide a review of the existing literature on this subject and propose an empirical expression for the rising velocity: $U_b = 0.323\sqrt{g\,(D_1 + D_2)}$, where D_1 and

D_2, respectively, stand for the internal and external diameter of the torus. This result can be compared to the law we propose $U_b = (8\pi)^{-1/2}\sqrt{gP}$, which, for a torus, can be written: $U_b \approx 0.35\sqrt{g(D_1 + D_2)}$. The structure is the same and the prefactors differ by only 8%. The results obtained by Sadatomi & Sato (1982) in toroidal tubes are presented in figure 8 and also follow the same dependency.

Although we have derived (4.20) only for rectangles and cylinders, this relation appears to be more general and accounts for the rising velocity of bubbles in vertical tubes of arbitrary cross-section, in the limit of high Reynolds and high Bond number. The pertinent length is found to be the total wetted perimeter of the tube and not the hydraulic radius.

4.2. *Taylor bubbles at low Reynolds and large Bond numbers*

The difficulty in the viscous regime is that the streamfunctions are not known and the method used in the previous section cannot be pursued. We thus approach the bubble velocity through dimensional analysis. The most instructive case is that of the rectangular channel, characterized by two independent length scales, R_x and R_z.

4.2.1. *Bubbles in rectangular channels*

For a bubble rising through a viscous liquid in a rectangular channel, the velocity results from a balance between buoyancy and viscous friction. For a unit bubble length, this balance can be written:

$$\rho g S \propto \mu \frac{U_b}{L} P, \tag{4.21}$$

where S and P are the surface and the perimeter. The length L is unknown and characterizes the distance on which the gradient of velocity is established. For a fixed surface, let us look at the limit $R_x/R_z \gg 1$. In this limit, P tends to $4R_x$.

If $L \propto R_z$, (4.21) implies that:

$$U_b \propto \frac{g R_z^2}{\nu}. \tag{4.22}$$

This is the typical scaling of the velocity in Hele-Shaw cells (Saffman & Taylor 1958).

If $L \propto R_x$, (4.21) implies that:

$$U_b \propto \frac{gS}{\nu}. \tag{4.23}$$

Both behaviours exist: figure 10(*a*) shows the evolution of the reduced velocity $U_b\nu/(gS)$ as a function of the aspect ratio $R_x/R_z \geqslant 1$. The data obtained with different liquids follow the same curve. The ranges of Reynolds numbers $Re_s \equiv U_b(S/P)/\nu$ associated with these data are: $Re_s[\mathrm{V1000}] \in [4 \times 10^{-4}, 0.3]$, $Re_s[\mathrm{V12500}] \in [2 \times 10^{-4}, 0.02]$, $Re_s[\mathrm{V100000}] \in [6 \times 10^{-5}, 5 \times 10^{-4}]$ and $Re_s[\mathrm{Glycerol}] \in [5 \times 10^{-3}, 0.5]$.

For small values of the aspect ratio, we see that $U_b\nu/(gS)$ is almost constant and equal to 0.012 ± 0.0005. For higher values of the aspect ratio, we reach the Hele-Shaw limit where $U_b\nu/(gS) \propto (R_x/R_z)^{-1}$. The transition between the two regimes occurs for $R_x/R_z \approx 7$.

4.2.2. *Bubbles in tubes of arbitrary cross-section*

If we use the section $S = \pi R^2$ of a cylindrical tube in the expression $U_b \approx 0.012 gS/\nu$ found for rectangles with aspect ratio smaller than 7, we find $U_b \approx 0.0377 gR^2/\nu$. This expression is close to the known value for cylinders, equation (1.2).

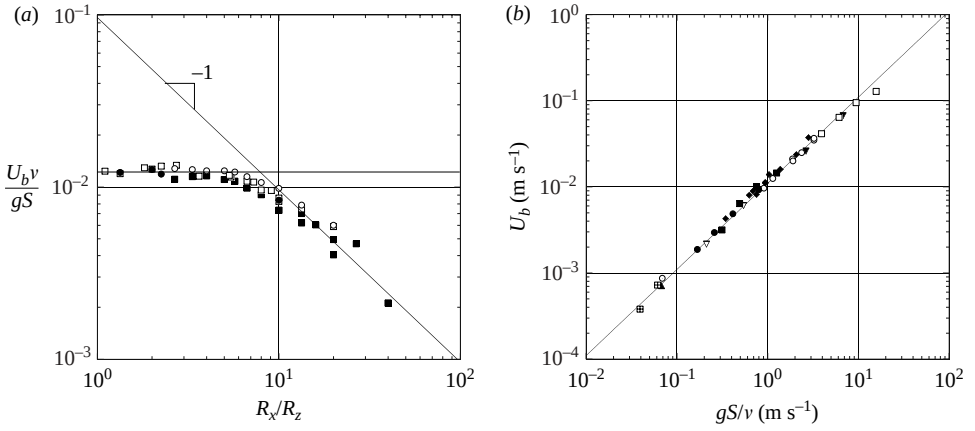

FIGURE 10. Experimental results at low Reynolds numbers: (*a*) in rectangles with different liquids: ■, SO V1000; □, SO V12500; ●, SO V100000; ○, glycerol; (*b*) in different shapes with the three silicone oils, V1000, V12500, V100000: ▼, ▽, ▲, three oils in triangles; □, ■, ⊞, three oils in squares; ○, ●, ⊙, three oils in circles; ◆, V12500 in rectangles, the solid line is the best fit $U_b = 0.012gS/\nu$.

We now examine the validity of this scaling law, gS/ν, for bubble velocity in tubes of arbitrary cross-section, but with a small aspect ratio. The results obtained for air bubbles in triangles, squares, circles and rectangles with an aspect ratio smaller than 7 are presented in figure 10(*b*). For the different shapes and liquids, we observe that the velocity of the bubble follows the universal law

$$U_b \approx 0.012gS/\nu.$$

This law applies in the low-Reynolds-number region, provided capillary effects can be neglected.

In the high-Reynolds-number region, we have shown in § 4.1 that $U_b = (8\pi)^{-1/2}\sqrt{gP}$. The transition between these two regions is presented in figure 11. The reduced velocity U_b^2/gP is presented as a function of the Reynolds number $Re_s \equiv U_b(S/P)/\nu$, based on the ratio of cross-section to perimeter. The data obtained in regular polygons (triangles, squares and circles) and rectangles with aspect ratio smaller than 7 clearly follow the same curve, over ten decades. The viscous region is described by $U_b^2/gP \approx 0.012Re_s$. This law is observed to apply in the range $Re_s \leqslant 1$. In the other limit, the inertial region is described by $U_b^2/gP = 1/(8\pi)$. This law holds when $Re_s \geqslant 100$. Looking at the crossing point of both laws, we see that the transition occurs at the critical Reynolds number $Re_s \approx 4$.

5. Unsteady dynamics of long bubbles in vertical tubes

In this section, we extend the model presented in § 4.1 to describe the dynamics of long bubbles in vertical cylindrical tubes submitted to an unsteady gravitational field. This was achieved experimentally by Brannock & Kubie (1996) by shaking vertical tubes with an amplitude A and a pulsation ω. To compare the predictions of our model to the results of Brannock & Kubie (1996) obtained with water in large tubes, we focus on the inertial regime without surface tension.

The frame of reference moving with the bubble is now non-Galilean. The Euler equation for the flow around the bubble can be written:

$$\frac{\partial \boldsymbol{U}}{\partial t} + \nabla \boldsymbol{U} \cdot \boldsymbol{U} = -\frac{1}{\rho}\nabla p + \boldsymbol{g} + \frac{\mathrm{d}U_b}{\mathrm{d}t}\boldsymbol{e}_y. \tag{5.1}$$

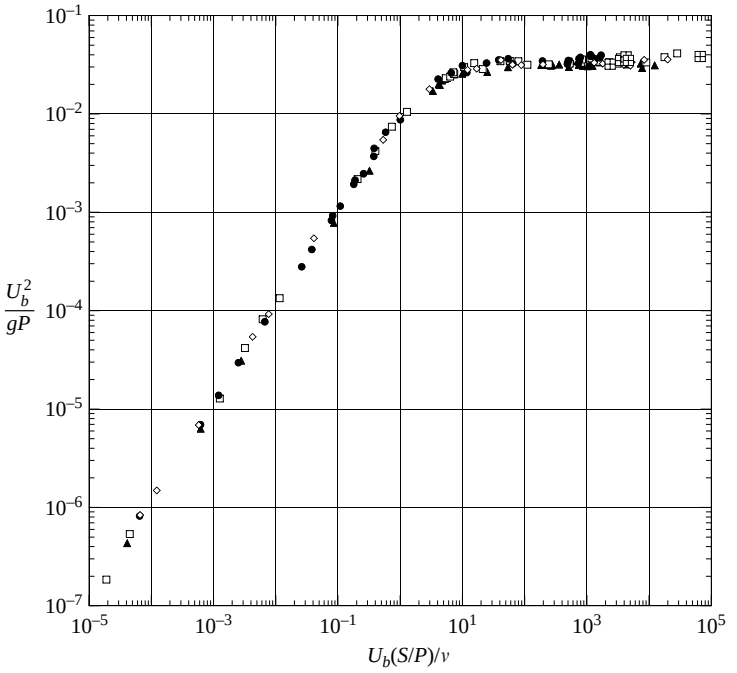

FIGURE 11. Experimental results for the bubble reduced velocity square U_b^2/gP as a function of the Reynolds number $U_b(S/P)\nu$ for tubes of different shapes. All the liquids presented in table 1 are used. For all the experiments, the Bond number is large. ▲, triangle; □, square; ●, circle; ◇, rectangles with aspect ratio smaller than 7; ⊞, toroidal tubes.

We look for a potential solution $\boldsymbol{U} = \nabla\Phi$ that satisfies the condition of constant pressure at the surface of the bubble. This condition leads to:

$$U^2 = 2\left[\left(g + \frac{\mathrm{d}U_b}{\mathrm{d}t}\right) y + \left.\frac{\partial\Phi}{\partial t}\right|_0 - \left.\frac{\partial\Phi}{\partial t}\right|_y\right]. \tag{5.2}$$

In the steady limit, (5.2) reduces to (4.1). For a long bubble in a cylindrical tube of radius R, we choose the potential:

$$\Phi = \frac{U_b(t)}{k_0}[k_0 y - \mathrm{e}^{k_0 y}\, J_0(k_0 r)], \tag{5.3}$$

where $k_0 R = 3.83$ satisfies the condition of zero normal velocity at the wall.

This evaluation of the velocity potential reduces the condition (5.2) to the ordinary differential equation:

$$\frac{\mathrm{d}U_b}{\mathrm{d}t} + k_0 U_b^2 - g(t) = 0. \tag{5.4}$$

In the steady limit, this differential equation reduces to the explicit value of the bubble velocity: $U_b^2 = g/k_0$ derived in (4.4). In the unsteady limit, we find that the bubble velocity is a function of time, related to the unsteady gravitational field $g(t)$ through the differential equation (5.4).

In the linear limit $g(t) = g_0(1 + \epsilon \mathrm{e}^{\mathrm{i}\omega t})$, we look for solutions $U_b(t) = U_{b0}(1 + \epsilon_u \mathrm{e}^{\mathrm{i}\omega t})$ and find:

$$\epsilon_u = \frac{\epsilon}{2}\frac{1}{1 + \mathrm{i}\omega\tau} \quad \text{with} \quad \tau = \frac{U_{b0}}{g_0} = \sqrt{\frac{R}{15.3 g_0}}. \tag{5.5}$$

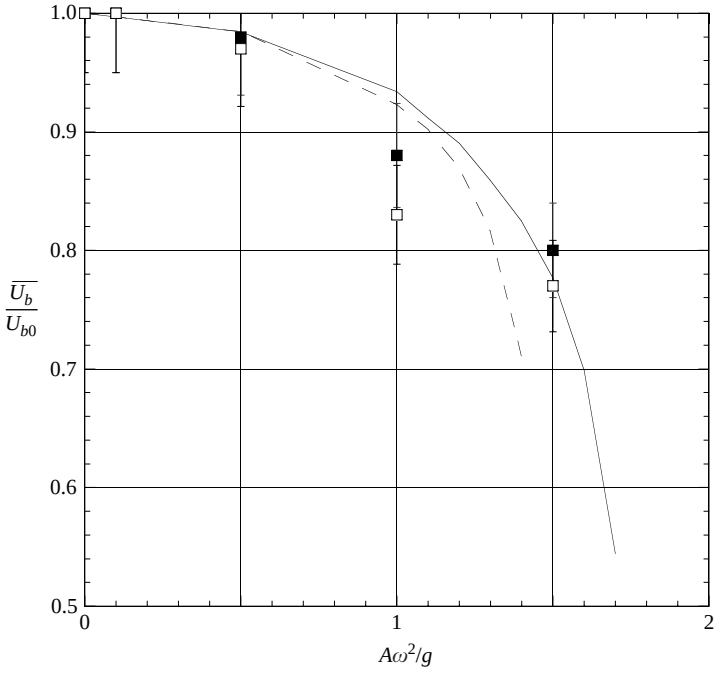

FIGURE 12. Comparison between the experimental results of Brannock & Kubie (1996) and the numerical integration of (5.4): ■, experiment ($R = 22$ mm); □, experiment ($R = 11$ mm); solid line ((5.4) with $R = 22$ mm); dashed line ((5.4) with $R = 11$ mm).

The long bubble thus behaves as a low-pass filter characterized by the cut-off frequency $1/\tau$.

For a periodical forcing, as the one imposed experimentally by Brannock & Kubie (1996), $g(t) = g + A\omega^2 \sin \omega t$, we can more generally decompose the velocity into a mean and fluctuating part: $U_b(t) = \overline{U_b} + \tilde{U}_b(t)$. Taking the average of the whole equation (5.4) leads to:

$$\overline{U_b^2} + \overline{\tilde{U}_b^2} = U_{b0}^2 . \tag{5.6}$$

Equation (5.6) shows that the mean velocity $\overline{U_b}$ decreases as $\overline{\tilde{U}_b^2}$ increases. The mean velocity reaches zero for $\overline{\tilde{U}_b^2} = U_{b0}^2$. This linear analysis leads to a critical acceleration $A\omega^2/g = \sqrt{8}$. In their experimental work, Brannock & Kubie indeed find that the bubble velocity decreases as $A\omega^2$ is increased. However, their critical acceleration is $A\omega^2/g \approx 1.6$. Our linear analysis is qualitatively correct, but the quantitative difference arises from the linearization of (5.4), which must be solved numerically.

In the experiment of Brannock & Kubie (1996), a vertical tube, 2 m long, is shaken vertically with a pulsation ω and an amplitude A, giving a reduced acceleration $A\omega^2/g$ increasing from 0 upto 1.5. From the time required to empty the tube T, the authors define the mean velocity $\bar{U}_b = L/T$ and present its evolution as a function of the reduced acceleration. Their results, non-dimensionalized by the steady velocity U_{b0}, are reported in figure 12 for two different radii. We also present in this figure the results obtained by the numerical integration of (5.4). The tendencies are correct. Moreover, we observe numerically that the bubble is stopped for a reduced acceleration of the order of 1.7. Experimentally, Brannock & Kubie report that for a reduced acceleration

of the order of 1.6, the bubble is broken. If the tip of the bubble is not stable, our model should not work. The comparison between the experiment and the model should be limited to the range of acceleration where the tip remains stable, and in this limit, according to figure 12, the predictions of the model are correct.

6. Conclusion

We have studied the steady propagation of long bubbles in vertical tubes of different forms and cross-sections. Considering air bubbles propagating through viscous and non-viscous liquids, contained in tubes of large cross-section, we have defined two domains, characterized by different dynamics and scaling parameters.

In the high-Reynolds-number limit, it is shown experimentally and analytically that, for all the tubes tested, $U_b = (8\pi)^{-1/2}\sqrt{gP}$, where P is the wetted perimeter of the cross-section of the tube. Similarly, in the low-Reynolds- and high-Bond-number limit we find $U_b \approx 0.012gS/\nu$, where S is the surface of the tube cross-section.

For all tubes and all liquids, the transition from high- to low-Reynolds-number regime is shown to occur at the critical value $Re_s \approx 4$, where $Re_s \equiv U_b(S/P)/\nu$ is the Reynolds number based on the ratio of cross-section to perimeter.

Finally, we have considered the case of unsteady bubble propagation obtained by shaking the tube vertically at different frequencies. A simple extension of our analytical potential model yields a differential equation for the determination of U_b. The results obtained both analytically and through a numerical integration predict a decrease of the mean velocity of the bubble and a cutoff value of the reduced acceleration beyond which the propagation of the bubble is blocked. These results are in good agreement with published experimental results.

This work is part of the PhD thesis of P. H., funded by the DGA (Délégation Générale de l'Armement) and the CTSN (Centre Technique des Systèmes Navals) A996111100. We thank J. Minelli, F. Abetino and F. Dutertre for their skilful technical assistance and for their meaningful comments and suggestions. We are also grateful to J. Magnaudet for his comments on the theory.

REFERENCES

Aussillous, P. & Quéré, D. 2000 Quick deposition of a fluid on the wall of a tube. *Phys. Fluids* **12**, 2367.

Bi, Q. C. & Zhao, T. S. 2001 Taylor bubbles in miniaturized circular and noncircular channels. *Intl J. Multiphase Flow* **27**, 561–570.

Bico, J. & Quéré, D. 2002 Rise of liquids and bubbles in angular capillary tubes. *J. Colloid Interface Sci.* **247**, 162–166.

Brannock, D. & Kubie, J. 1996 Velocity of long bubbles in oscillating vertical pipes. *Intl. J. Multiphase Flow* **22**, 1031–1034.

Bretherton, F. P. 1961 The motion of long bubbles in tubes. *J. Fluid Mech.* **10**, 166–188.

Bugg, J. D. & Saad, G. A. 2002 The velocity field around a Taylor bubble rising in a stagnant viscous fluid: numerical and experimental results. *Intl J. Multiphase Flow* **28**, 791–803.

Daripa, P. 2000 A computational study of rising plane Taylor bubbles. *J. Comput. Phys.* **157**, 120–142.

Das, G., Das, P. K., Purohit, N. K. & Mitra, A. K. 1998 Rise velocity of a Taylor bubble through concentric annulus. *Chem. Engng Sci.* **53**, 977–993.

Das, G., Purohit, N. K., Mitra, A. K. & Das, P. K. 2002 Geometry of Taylor bubbles rising through liquid-filled annuli. *AIChE J.* **48**, 411–416.

Davies, R. M. & Taylor, G. I. 1950 The mechanics of large bubbles rising through extended liquids and through liquids in tubes. *Proc. R. Soc. Lond.* A **200**, 375–390.

Dumitrescu, D. T. 1943 Strömung an einer Luftblase im senkrechten Rohr. *Z. Angew. Math. Mech.* **23**, 139–149.

Fabre, J. & Liné, A. 1992 Modelling of two-phase slug flow. *Annu. Rev. Fluid Mech.* **24**, 21–46.

Fulford, G. D. 1964 The flow of liquids in thin films. *Adv. Chem. Engng* **5**, 151–236.

Garabedian, P. R. 1957 On steady state bubbles generated by Taylor instability. *Proc. R. Soc. Lond.* A **241**, 423.

Griffith, P. 1964 The prediction of low-quality boiling voids. *Trans. ASME: J. Heat Transfer* **86**, 327–333.

Haberman, W. L. & Morton, R. K. 1956 An experimental study of bubbles moving in liquids. *Trans. Am. Soc. Civil Engng* **121**, 227–252.

Hazel, A. L. & Heil, M. 2002 The steady propagation of a semi-infinite bubble into a tube of elliptical or rectangular cross-section. *J. Fluid Mech.* **470**, 91–114.

Hills, J. H. & Chety, P. 1998 The rising velocity of Taylor bubbles in an annulus. *Chem. Engng Res. Des.* **76**, 723–727.

van Hout, R., Gulitski, A., Barnea, D. & Shemer, L. 2002 Experimental investigation of the velocity field induced by a Taylor bubble rising in stagnant water. *Intl J. Multiphase Flow* **28**, 579–596.

Kapitsa, P. L. 1948 Wave flow of thin layers of a viscous fluid. *Zh. Eksperim. Teor. Fiz.* **18**, 59–129.

Kolb, W. B. & Cerro, R. L. 1991 Coating the inside of a capillary of square cross-section. *Chem. Engng Sci.* **46**, 2181–2195.

Kolb, W. B. & Cerro, R. L. 1993 Film flow in the space between a circular bubble and a square tube. *J. Colloid Interface Sci.* **159**, 302–311.

Kolb, W. B. & Cerro, R. L. 1995 The motion of long bubbles in tubes of square cross-section. *Phys. Fluids* **7**, 1549.

Layzer, D. 1955 On the instability of superposed fluids in a gravitational field. *Astrophys. J.* **122**, 1–12.

Liao, Q. & Zhao, T. S. 2003 Modeling of Taylor bubble rising in a vertical mini noncircular channel filled with a stagnant liquid. *Intl J. Multiphase Flow* **29**, 411–434.

Park, C. W. & Homsy, G. M. 1984 Two-phase displacement in Hele Shaw cells: theory. *J. Fluid Mech.* **139**, 291–308.

Ratulowski, J. & Chang, H. C. 1989 Transport of gas bubbles in capillaries. *Phys. Fluids* A **1**, 1642–1655.

Reinelt, D. A. 1987 The rate at which a long bubble rises in a vertical tube. *J. Fluid. Mech.* **175**, 557–565.

Reinelt, D. A. & Saffman, P. G. 1985 The penetration of a finger into a viscous fluid in a channel and tube. *SIAM J. Sci. Statist. Comput.* **6**, 542–561.

Sadatomi, M. & Sato, Y. 1982 Two-phase flow in vertical noncircular channels. *Intl J. Multiphase Flow* **8**, 641–655.

Saffman, P. G. & Taylor, G. I. 1958 The penetration of a fluid into a porous medium or Hele-Shaw cell containing a more viscous liquid. *Proc. R. Soc.* A **245**, 312–329.

Taylor, G. I. 1961 Deposition of a viscous fluid on the wall of a tube. *J. Fluid Mech.* **10**, 161.

White, E. T. & Beardmore, R. H. 1962 The velocity of rise of single cylindrical air bubbles through liquids contained in vertical tubes. *Chem. Engng Sci.* **17**, 351–361.

Wong, H., Radke, C. J. & Morris, S. 1995*a* The motion of long bubbles in polygonal capillaries. Part 1. Thin films. *J. Fluid Mech.* **292**, 71–94.

Wong, H., Radke, C. J. & Morris, S. 1995*a* The motion of long bubbles in polygonal capillaries. Part 2. Drag, fluid pressure and fluid flow. *J. Fluid Mech.* **292**, 95–110.

Zel'dovich, Ya. B., Istratov, A. G., Kidin, N. I. & Librovich, V. B. 1980 Flame propagation in tubes: hydrodynamics and stability. *Combust. Sci. Technol.* **24**, 1–13.

Zukoski, E. E. 1966 Influence of viscosity, surface tension, and inclination angle on motion of long bubbles in closed tubes. *J. Fluid Mech.* **25**, 821–837.